


Locally Resonant Metasurfaces for Shear Waves in Granular Media

Rachele Zaccherini^{1,*}, Andrea Colombi¹, Antonio Palermo², Vasilis K. Dertimanis¹,
Alessandro Marzani², Henrik R. Thomsen³, Bozidar Stojadinovic¹, and Eleni N. Chatzi¹

¹*Department of Civil, Environmental and Geomatic Engineering, ETH Zürich, Zürich 8093, Switzerland*

²*Department of Civil, Chemical, Environmental and Materials Engineering—DICAM, University of Bologna, Bologna 40136, Italy*

³*Department of Earth Sciences, ETH Zürich, Zürich 8092, Switzerland*

 (Received 31 October 2019; revised manuscript received 9 February 2020; accepted 4 March 2020; published 23 March 2020)

In this paper, the physics of horizontally polarized shear waves traveling across a locally resonant metasurface in an unconsolidated granular medium is experimentally and numerically explored. The metasurface is comprised of an arrangement of subwavelength horizontal mechanical resonators embedded in a granular layer made of silica microbeads. The metasurface supports a frequency-tailorable attenuation zone induced by the translational mode of the resonators. The experimental and numerical findings reveal that the metasurface not only backscatters part of the energy but also redirects the wave front underneath the resonators, leading to a considerable amplitude attenuation at the surface level, when all the resonators have similar resonant frequency. A more complex picture emerges when using resonators arranged in a so-called graded design, e.g., with a resonant frequency increasing or decreasing throughout the metasurface. Unlike the mechanism observed in a bilayered medium, shear waves localized at the surface of the granular material are not converted into bulk waves. Although a detachment from the surface occurs, the depth-dependent velocity profile of the granular medium prevents the mode conversion and the horizontally polarized shear wave front returns to the surface. The outcomes of our experimental and numerical studies allow for understanding the dynamics of wave propagation in resonant metamaterials embedded in vertically inhomogeneous soils and, therefore, may be valuable for improving the design of engineered devices for ground-vibration and seismic wave containment.

DOI: [10.1103/PhysRevApplied.13.034055](https://doi.org/10.1103/PhysRevApplied.13.034055)

I. INTRODUCTION

Years of study on artificial periodic and locally resonant media for electromagnetic [1,2], acoustic [3,4], and elastic [5,6] wave control have laid the foundation for the broad application of these structures, known as metamaterials, across several fields and scales. Of particular interest in the context of elastodynamics are metamaterials comprised of subwavelength-resonant elements [7], since they feature spectral band gaps (i.e., a frequency range of inhibited wave transmission) at low frequencies and, contrary to phononic crystals, they do not rely on periodicity [8–10]. The ability to mitigate waves and vibrations through the use of resonance-induced band gaps has been exploited in the context of vibration mitigation in numerous mechanical- and civil-engineering practical problems, where a surge of metamaterial designs has been proposed [11–13]. Despite the differences in terms of the size and targeted frequency, the majority of the proposed designs rely on the coupling between a structural component (a beam [14,15] or a plate [16–18]) and an

array of mechanical resonators. The coupling occurring between the resonators and the waves propagating inside the component induces a band gap in the subwavelength regime [19]. In civil engineering, for instance, arrays of meter-large mechanical resonators embedded in the soil surface, typically referred to as elastic metasurfaces [20] or integrated in the building's foundations [21,22], have recently been proposed with the aim of shielding infrastructures from ground-borne vibrations and possibly even seismic waves.

While shielding is effective inside the band gap, the corresponding bandwidth is generally too narrow to cover the wide frequency content of incoming waves. Some of the strategies devised to enlarge the band gap entail the use of nonlinear resonators [23] and, as also discussed in this paper, the implementation of a graded design, i.e., an array of resonators with a spatially varying resonant frequency [24]. The theory behind metasurfaces and graded metasurfaces is well established for simple mechanical systems such as plates [25], waveguides [26,27], and half-spaces [28] when Lamb or vertically polarized (e.g., Rayleigh-like) waves are considered. Conversely, only a handful of numerical papers have investigated the behavior

*zaccherini@ibk.baug.ethz.ch

of metasurfaces interacting with horizontally polarized surface waves. Among these, two studies [29,30] have considered the interaction between Love waves [31] and mechanical oscillators placed at the free surface of a soft layer overlying a homogeneous elastic half-space. However, actual soils rarely exhibit a bilayer structure and research considering more complex and realistic media is necessary.

In geophysics, a well-established experimental approach uses unconsolidated granular media [32] to mimic an inhomogeneous soil featuring a depth-dependent velocity gradient. The stiffness profile of such media exhibits a power-law dependence on the compacting pressure along the depth [33–35]. Similar depth dependencies are often also adopted in geotechnical studies [36,37].

In unconsolidated granular media, the inherent gravity-induced stiffness gradient, which causes an upward bending of the rays [38], combined with the presence of a free surface, enables the propagation of low-velocity guided surface acoustic modes (GSAMs). These GSAMs, confined between the surface and the in-depth layer with increasing rigidity, include shear horizontal (SH) waves and vertically polarized (P-SV) waves composed of continuously interacting longitudinal (P) and shear vertical (SV) components. A recent study [20] has investigated the interaction of the P-SV acoustic modes with a metasurface of vertical oscillators. The findings have revealed the hybridization of the lowest-order P-SV wave at the metasurface resonance but an absence of surface-to-bulk mode conversion observed in homogeneous half-spaces, ascribable to the stiffness profile of the granular medium.

In this work, we extend the analysis to the dynamics of SH modes, the existence of which has been analytically predicted [33,34] but is yet to be experimentally observed, offering insights into their interaction with a metasurface of subwavelength horizontal oscillators. By carrying out a small-scale experiment at the IBK Laboratory of ETH Zürich, we demonstrate how SH waves propagate through a resonant metasurface embedded in a micrometric granular medium. We then validate the findings by means of dispersion-curve analysis and three-dimensional (3D) time-transient numerical simulations. To distinguish between Bragg scattering and local resonance phenomena, we measure the SH wave field within an array of plastic casings buried under the medium surface (here dubbed the “nonresonant casings surface”) and compare this with the measurements inside the resonant metasurface. Finally, we numerically and experimentally study the interaction between surface SH waves and a graded metasurface of increasing and decreasing frequency. Our findings allow for understanding the dynamics of wave propagation in resonant metamaterials embedded in soils with an inhomogeneous power-law elastic profile and, therefore, may be valuable for improving the design of engineered devices for ground-vibration and seismic wave containment.

II. RESULTS

A. Experimental setup and data acquisition

The experimental setup shown in Fig. 1(a) includes a wooden box ($2000 \times 1500 \times 1000$ mm) filled with granular material (150- μm -diameter glass beads with density of 1600 kg/m^3), a Polytech PSV-500 3D laser Doppler vibrometer, capable of recording the velocity field along three normal directions, and a Physik Instrumente three-axis piezoelectric actuator driven by a PiezoDrive amplifier. The dimensions of the box are chosen to minimize the interaction between the primary signal and reflections generated by the lateral and bottom surfaces within the time window of interest. In addition, to mitigate the amplitude of the reflected signals, a paperboard layer is placed at the base of the box. Similar experimental setups have been used to study the propagation of vertically polarized seismic waves in unconsolidated and porous media [32,39–41] and to investigate their interaction with a metasurface of vertical oscillators [20]. The granular material is gently poured and leveled to ensure a uniform compaction and the realization of a planar surface. The piezoelectric actuator, fixed to a steel block ($150 \times 100 \times 40$ mm) buried at 20-mm depth, excites the granular material, generating elastic waves polarized in the horizontal plane (SH waves) and localized near the surface. To do this, we only activate the piezoelectric stack corresponding to the y axis [Fig. 1(a)]. As input signals [Fig. 1(a)], we employ both a modulated chirp from 100 to 800 Hz, which is useful to derive the dispersion properties, and a Ricker wavelet centered at 300 Hz to realize a pulselike excitation. To limit the effect of nonlinearities between the actuator and the granular material, the maximum displacement excursion of the actuator is kept below $2 \mu\text{m}$.

The metasurface is built by embedding 48 subwavelength mechanical oscillators at the surface of the granular medium. Each resonator consists of a squared mass (of 10.2 g) supported by four ligaments, which prevent vertical motion, four horizontal trusslike springs, and an external casing [height 22 mm, width 20 mm; see Fig. 1(b)]. The resonator casing and connectors are 3D printed in versatile plastic ($E = 1700 \text{ MPa}$, $\nu = 0.3$, and $\rho = 450 \text{ kg/m}^3$) using the selective-laser-sintering technique, which allows the fabrication of the horizontal springs with no need for material support. The resonating mass (height 10 mm, side 10 mm) is made out of brass. The resonant frequency of the mechanical oscillators can be tailored by adjustment of the inclination angle and length of the beams forming the trusslike springs. By design, we set the horizontal resonant frequency of the generic resonator, accounting for the coupling with the surrounding granular material, at $f_r = 330 \text{ Hz}$. This resonance value is chosen after experimentally identifying the frequency content of the SH modes propagating in the pristine granular medium, in order to observe potential hybridization phenomena in a

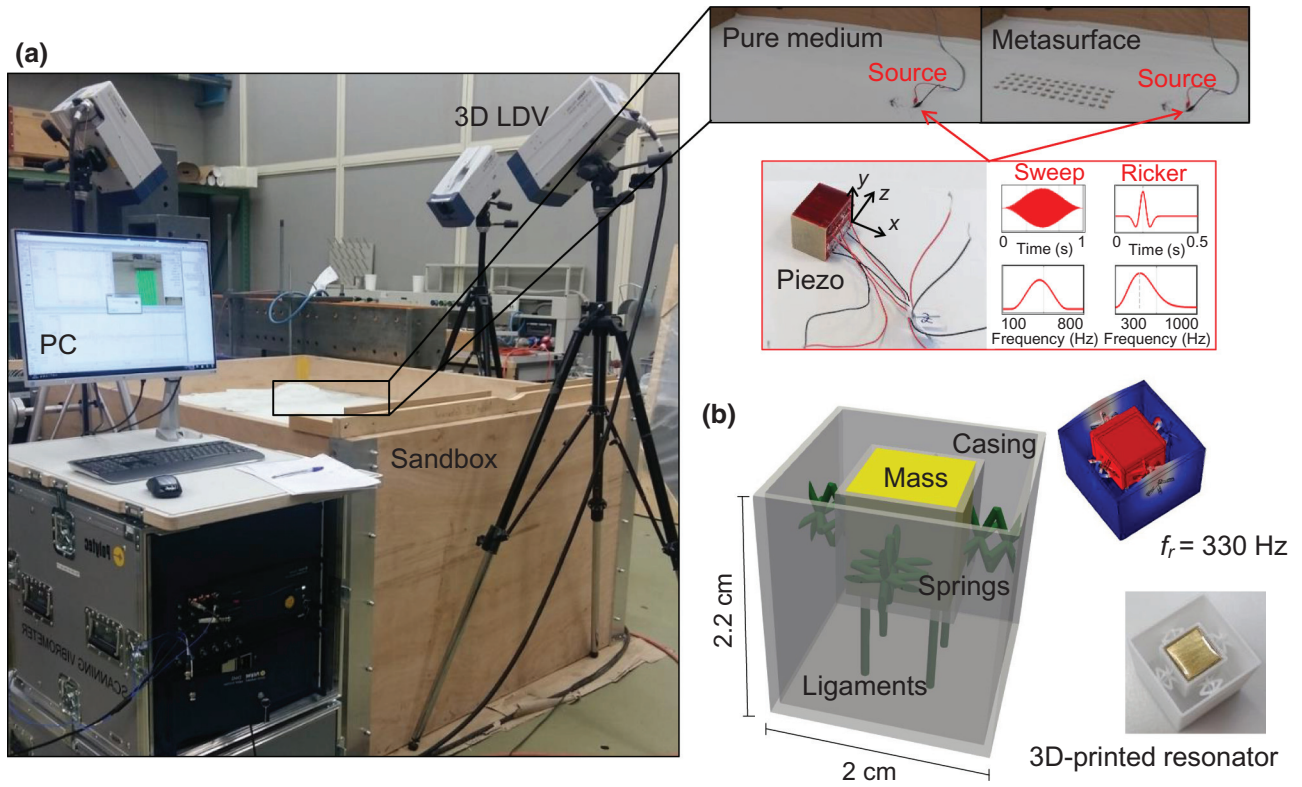


FIG. 1. The experimental setup and mechanical resonators. (a) The experimental setup, involving a wooden box filled with granular material, a 3D laser Doppler vibrometer, an array of subwavelength horizontal oscillators and a three-axis piezoelectric actuator. (b) A model of the elementary unit cell, including a squared brass mass, four trusslike springs, four ligaments acting as vertical supports, and an outer casing. The first translational mode of the resonant unit together with an illustration of the assembled 3D-printed resonator.

frequency range in which the waves are highly excited. We experimentally validate this resonance by exciting the oscillators with the piezoelectric actuator. The metasurface is then obtained by arranging the resonators on the medium surface in a 4×12 rectangular grid [see Fig. 1(a)].

For the graded metasurfaces, oscillators with different masses (of 7, 9.1, 10.2, and 13.3 g, respectively) are fabricated. In particular, we assemble four different types of resonators ($f_{r1} = 250$ Hz, $f_{r2} = 320$ Hz, $f_{r3} = 330$ Hz, and $f_{r4} = 360$ Hz) and arrange them according to increasing and decreasing frequencies. In addition, a nonresonant surface is realized by embedding an identical 4×12 arrangement of resonator casings, hosting an internal brass mass with no springs. For all adopted configurations, i.e., pristine granular surface, metasurfaces, and nonresonant casings, we use the 3D vibrometer to scan the surface velocity of the granular medium both along the symmetry axis of the box with a constant step of $\Delta x = 7$ mm and over a 380×650 mm area with constant spatial steps of $\Delta x = \Delta y = 12$ mm. For each acquisition point, we average ten signals of 0.5 s duration at a sampling rate of 5 kHz.

B. Dispersion analysis of the metasurface

The two-dimensional (2D) discrete Fourier transforms (DFTs) of the velocity data recorded along the central

horizontal line and representing the dispersion curves are depicted in Figs. 2(a) and 2(b). For the reference case (i.e., the pristine granular material without resonators) the fundamental SH_1 and the second higher-order SH_2 mode can be clearly identified [Fig. 2(a)]. While the fundamental mode dominates the spectrum from 200 to 500 Hz with lower velocities (approximately 60 m/s), SH_2 prevails at higher frequencies, traveling at a higher velocity (approximately 80 m/s). Figure 2(b) shows the dispersion curves extracted within the resonant metasurface. The SH_1 mode interacts with the collective resonances of the metasurface, yielding a classical hybridization mechanism between the propagating surface wave and the standing mode of the metasurface. This coupling results in a flat mode (here labeled “ SH_{1m} ,” where “ m ” stands for metasurface), which converges asymptotically to the oscillator resonance frequency. Indeed, the dynamics of this SH_{1m} mode resemble that observed for the Love fundamental mode propagating in a bilayered medium and interacting with a metasurface of horizontal oscillators [29]. Since the smallest wavelength of the SH waves at the resonance $f_r = 330$ Hz (approximately 6 cm) is more than six times larger than the resonator spacing (1 cm), Bragg scattering should not play a role. This is confirmed in Fig. 2(c), where the 2D DFT of the velocity data is computed for the case

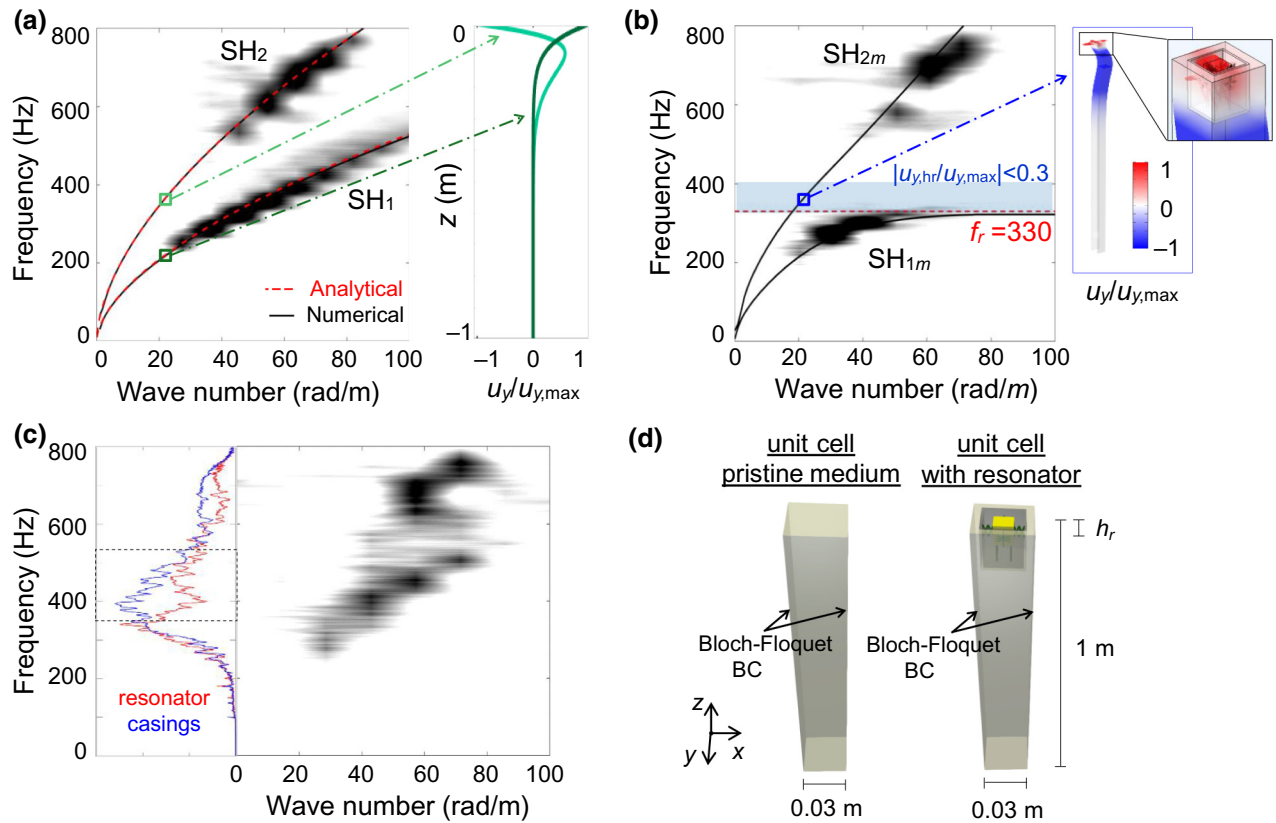


FIG. 2. Dispersion analysis. (a) The experimental, numerical (black line), and analytical (red dashed line) dispersion curves of the first two low-order SH modes localized at the surface of the granular medium, together with the corresponding shape modes for a value of $k = 20$ rad/m. (b) The experimental and numerical (black line) dispersion curves of the first two low-order SH modes propagating through the resonant metasurface, together with the shape mode of SH_{2m} for a value of $k = 20$ rad/m. The shaded light-blue area identifies the frequency range in which the surface displacement is negligible. This is defined as $|u_{y,hr}/u_{y,max}| < 0.3$, where $u_{y,hr}$ is the shear horizontal displacement calculated at the resonator embedding depth h_r and $u_{y,max}$ is the maximum displacement along the depth. (c) Experimental dispersion curves of SH waves propagating through the nonresonant casings surface. The lateral inset shows the average particle velocity measured in the frequency domain after one line of resonators (red line) and after one line of casings (blue line). (d) A drawing of the 3D unit cells with and without the resonators developed in COMSOL MULTIPHYSICS®.

in which the resonators are replaced with the nonresonant casings, equipped with internal masses equivalent to those of the resonators. The two SH modes are similar to the SH_1 and SH_2 observed in the reference case of Fig. 2(a). No hybridization and no band gap occur. The inset on the left depicts the average particle velocity measured in the frequency domain after one line of resonators (red line) and after one line of casings (blue line). Prior to reaching the resonant frequency of the oscillators (330 Hz), the two signals are similar. After 330 Hz, the particle velocity within the metasurface presents a dip inside the band-gap frequency range, centered around 400 Hz. This result confirms that the attenuation zone detected in Fig. 2(b) can be ascribed to the resonant behavior of the metasurface. We further verify that the effect of the dilatancy [42] (the volume change in granular media when subjected to shear deformations) does not significantly affect our analysis, since the amplitude of the longitudinal waves, both in the reference and metasurface case, is negligible compared

to that of the shear ones over the whole frequency range considered.

We now numerically investigate the dispersive properties of SH waves traveling both at the surface of the granular material and within the metasurface using a Bloch wave-finite element (FE) approach [43]. In particular, the dispersive analysis is numerically carried out by modeling a 3D FE model of the unit cell with and without the resonator [see Fig. 2(d)]. To obtain the Bloch-form wave solution, the velocity profile of the granular medium along the depth is required. Since closed-form solutions of the eigenvalue problem are available for SH waves in granular media [33], we use the analytical equation of the dispersion relation to estimate the velocity wave profile. This solution has been obtained by studying the dynamics of SH waves traveling in granular media using the GSAM theory described in Ref. [33], where the granular medium is considered as a linear elastic continuum. The theoretical compressional-velocity v_c and shear-velocity v_s

profiles of the granular medium are modeled with a power-law dependency on the compacting pressure p along the depth z : $v_{c,s} = \gamma_{c,s}(p)^{\alpha_{c,s}} = \gamma_{c,s}(\rho g z)^{\alpha_{c,s}}$, where ρ is the medium density, g is the gravitational constant, and $\gamma_{c,s}$, $\alpha_{c,s}$ represent the power-law parameters.

In the GSAM framework, the scalar displacement field associated with the SH modes, localized at the surface, $u_y = u_y(z)$, can be described via a depth-dependent Helmholtz equation:

$$[v_s^2(z)u_y'] + [(f/2\pi k)^2 - v_s^2(z)]u_y = 0, \quad (1)$$

where k and f are the wave number and the frequency, respectively. The governing equation is complemented with the following boundary conditions:

$$v_s^2(z)u_y'(z)|_{z=0} = 0, \quad u_y(z)|_{z \rightarrow \infty} = 0, \quad (2)$$

where the first one corresponds to the absence of shear stress σ_{zy} at the surface and the second one ensures that waves vanish toward depth. Substitution of Eq. (2) into (1) yields the SH-wave characteristic equation, which is analytically solved by applying the geometrical acoustic method [33]. The resulting eigenvalues are

$$\Omega_n^2 = \left\{ \pi \left[2n - 1 - \frac{2\alpha_s - 1}{2\alpha_s - 2} \right] \times \alpha_s \frac{\Gamma[(1/\alpha_s + 2)/2]}{\Gamma[(1/\alpha_s - 1)/2]\Gamma(3/2)} \right\}^{2\alpha_s}, \quad (3)$$

where Γ represents the Gamma function and the integer n is the n th-order mode.

Once the eigenvalues are obtained, the dispersion curve of the n th shear horizontal mode can be analytically expressed as follows:

$$f = \frac{\Omega_n \gamma_s (\rho g)^{\alpha_s} k^{1-\alpha_s}}{2\pi}. \quad (4)$$

By fitting the experimental dispersion curve of the fundamental SH wave (SH₁) using Eqs. (3) and (4), the power-law parameters for the shear profile are derived as $\alpha_s = 0.42$ and $\gamma_s = 3.82$. The compressional velocity profile, which does not affect the SH-wave propagation [see Eq. (1)] or the resonator, is derived assuming a Poisson ratio of $\nu = 0.376$, as in Ref. [33].

The velocity profiles are then inserted in the 3D unit cell FE models with and without the resonator, developed in COMSOL MULTIPHYSICS[®]. Indeed, the insertion of an object in a granular layer could change its compacting pressure and, consequently, induce a variation in the rigidity profile of the medium. However, since the resonator mass

(12.8 g) is similar to that of the displaced sand (14.1 g), the changes induced in the velocity profile are negligible. Hence, the same velocity profile is used to define the elastic properties of the granular medium in both FE models, with and without the resonator. The 3D granular unit cell is 1 m high and 0.03 m \times 0.03 m wide. The resonator model embedded in the granular material features the same geometric and material properties (mass, stiffness, and resonant frequency) as the 3D-printed mechanical oscillators. The medium, modeled as a linear elastic continuum, is defined through its density (constant) and velocity profiles (depth-dependent). For both the reference and the metasurface case, absorbing conditions are applied at the bottom edge and periodic Bloch-Floquet boundary conditions on the lateral faces. We perform an eigenfrequency analysis by sweeping the wave vector in the range $0 - k_{\max}$ (with $k_{\max} = \pi/D = 105$ rad/m) to obtain the numerical-dispersion relations. We observe an infinite number of SH modes with increasing phase velocity and, consequently, increasingly deep penetration into the medium, as further confirmed in recent studies [33,34]. Figure 2(a) depicts the numerical-dispersion curves of the first two SH modes (black lines), which overlap with the analytical ones (red dashed lines), as derived from Eq. (4), for the reference case. Furthermore, these numerical-dispersion relations are in good agreement with the experimental curves. The inset in Fig. 2(a) illustrates the mode shapes for SH₁ and SH₂ for a value of $k = 20$ rad/m. The maximum displacement occurs at the surface consistently for any surface mode. Moreover, the number of ‘‘phases’’ in the shear-displacement profile as a function of the depth corresponds to the order of the modes, as revealed in Ref. [33,34]. Figure 2(b) shows the numerical-dispersion curves of the first two SH modes interacting with the resonant metasurface (black lines). The hybridization between the local resonances and the fundamental mode is confirmed by the numerical analysis. Although a frequency gap does not occur, meaning that higher-order SH waves do not hybridize with the mechanical oscillators, the particle displacement of the surface layer enclosing the resonators is close to zero. The maximum horizontal displacement is now localized under the resonator [see the inset in Fig. 2(b)], suggesting possible SH-wave propagation under the resonant metasurface. The shaded light-blue area of Fig. 2(b) identifies the frequency range in which the surface displacement is negligible. This is defined as $u_{y,h_r}/u_{y,\max} < 0.3$, where u_{y,h_r} is the shear horizontal displacement calculated at the resonator embedding depth h_r [i.e., at the height of the center of gravity of the resonant mass; see Fig. 2(d)] and $u_{y,\max}$ is the maximum displacement along the depth. The existence of this frequency zone of quasizero displacement detected in proximity to the resonant frequency of the metasurface explains the energy gap observed in the experimental dispersion relation obtained from surface-velocity signals [Fig. 2(b)].

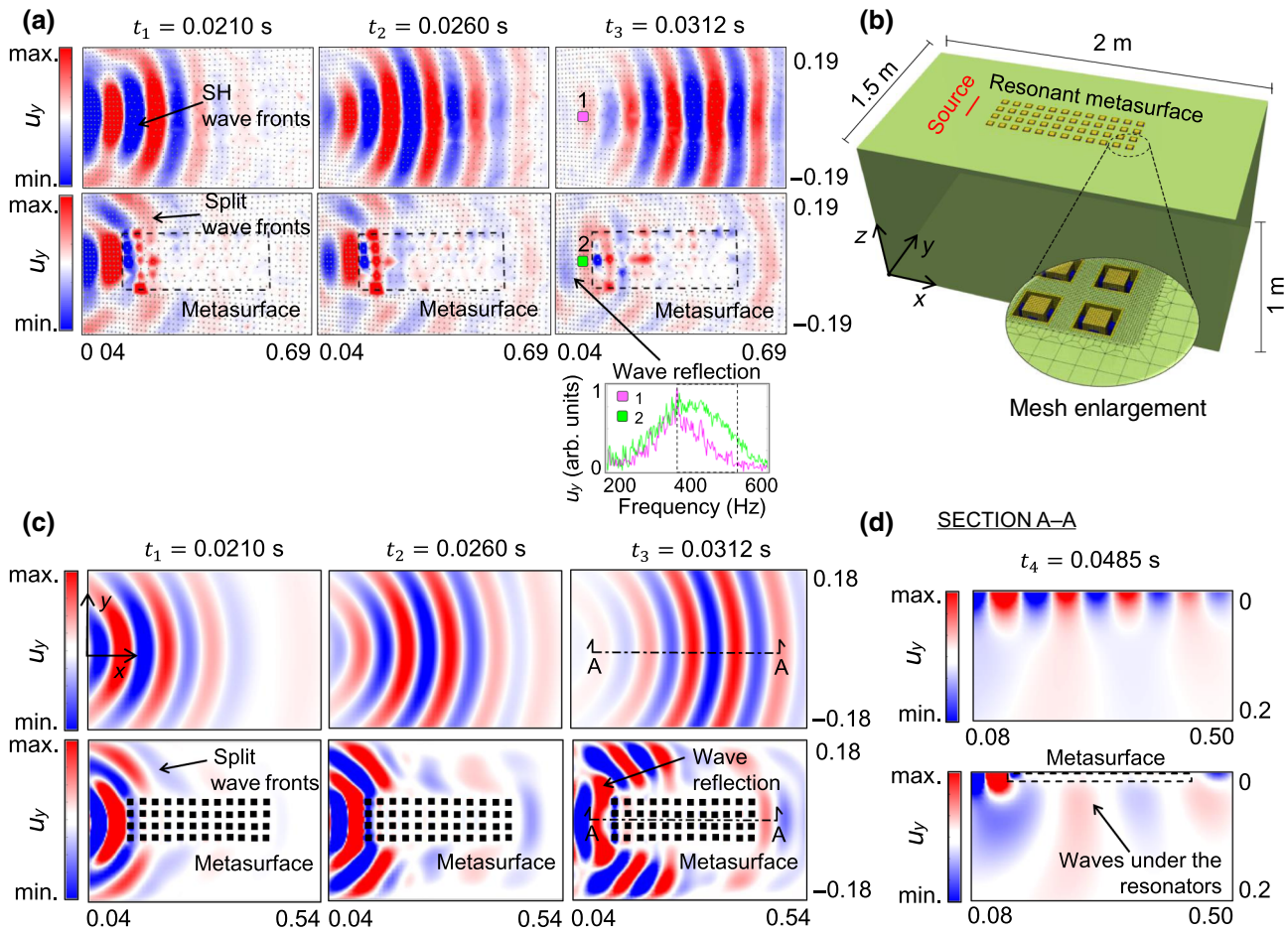


FIG. 3. The experimental and numerical displacement field with and without the metasurface. (a) The experimental displacement field of SH waves propagating at the free surface of the granular medium (top snapshots) and through the resonant metasurface (bottom snapshots) at three sequential time instants ($t_1 = 0.0210$ s, $t_2 = 0.0260$ s, and $t_3 = 0.0312$ s). (b) The computational domain characterized by the granular substrate and the resonant metasurface excited by a Ricker pulse centered at 300 Hz. The inset shows an enlargement of the adaptive mesh. (c) The numerical displacement field of SH waves propagating at the free surface of the granular medium (top snapshots) and through the resonant metasurface (bottom snapshots) at three sequential time instants ($t_1 = 0.0210$ s, $t_2 = 0.0260$ s, and $t_3 = 0.0312$ s). (d) Vertical cross sections through the center of the model, showing the numerical displacement field of SH waves traveling at the free surface (top snapshots) and through the metasurface (bottom snapshots) at $t_4 = 0.0485$ s.

C. Wave-field analysis in the metasurface

The experimental displacement fields of SH waves propagating at the free surface and within the resonant metasurface filtered inside the band gap (330–500 Hz) are compared at three sequential time instants ($t_1 = 0.0210$ s, $t_2 = 0.0260$ s, and $t_3 = 0.0312$ s) in Fig. 3(a). For the reference case without the resonators (top snapshots), nearly plane SH wave fronts propagate in the granular material. Conversely, when traveling within the metasurface (bottom snapshots), the SH wave fronts impinging on the mechanical oscillators are scattered and attenuated. The inset focuses on the displacement spectrum of a point on the surface located before the first resonator line in the reference case (point 1, purple line) and in the metasurface case (point 2, green line). The comparison between the two

signals reveals the frequency content of the reflected signal, which mainly falls inside the band gap. Although of low intensity, reflected wave fronts due to local resonances are visible in front of the metasurface in the third bottom snapshot at $t_3 = 0.0312$ s.

To verify these experimental observations and analyze the anatomy of the SH wave field interacting with the resonators, we perform 3D time-domain numerical simulations with and without the metasurface using SPEC3D, a parallel code based on the spectral-element method and able to solve large-scale time-dependent elastodynamic problems. The computational domain, depicted in Fig. 3(b), is a 1-m-deep half-space of granular medium, 2×1.5 m wide, modeled as a linear elastic continuum described by the previously estimated power-law velocity

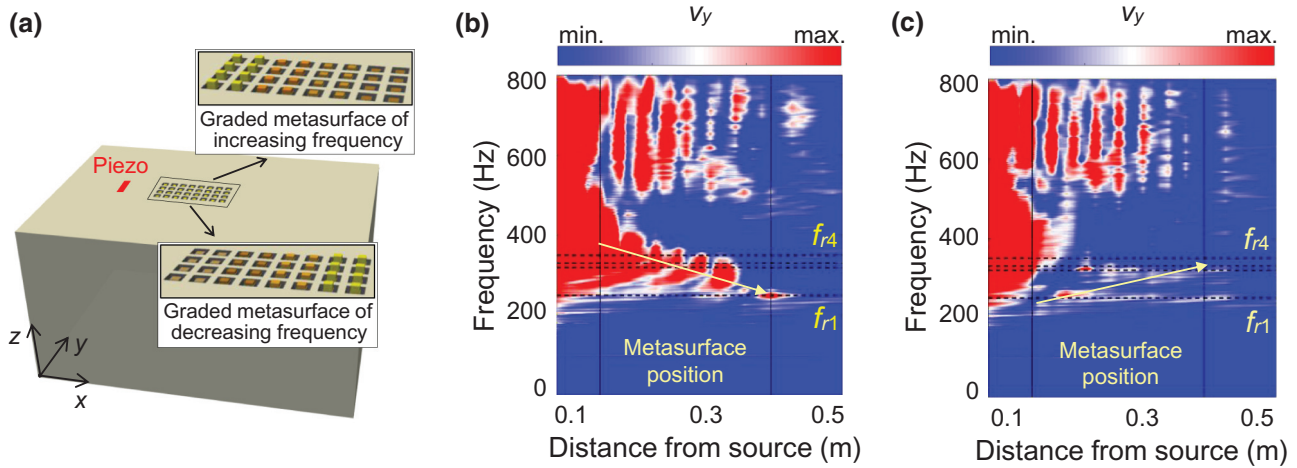


FIG. 4. The experimental velocity field within graded metasurfaces. (a) An outline of the experimental domain with resonant metasurfaces of gradually increasing and decreasing frequency. (b) The experimental particle velocity as a function of the frequency and the distance from the source for the case of a graded metasurface of decreasing frequency. (c) The same as (b) but for a graded metasurface of increasing frequency.

profile. While the upper surface of the domain is traction free to support surface-wave propagation, absorbing conditions are applied to the other boundaries to avoid reflections from the bottom and side edges of the box. A line source, applied at a distance of 0.2 m from the left boundary, is used to generate SH waves. The time history of the excitation is described by a Ricker pulse centered at 300 Hz. The metasurface comprises 48 resonators arranged in a 4×12 rectangular grid and featuring the properties (mass, stiffness, and resonant frequency) specified for the 3D-printed mechanical oscillators. An adaptive mesh of hexahedral elements, generated using the commercial software TRELIS 16.5 through PYTHON scripting, is adopted to speed up the computational cost of the simulations and to avoid distorted elements. The inset shows the fine mesh required to accurately model the tiny resonator structure. A 3D model of identical properties without the metastructure is used for the reference case.

Figure 3(c) shows the shear horizontal displacement field of harmonic SH waves traveling at three different time instants ($t_1 = 0.0210$ s, $t_2 = 0.0260$ s, and $t_3 = 0.0312$ s) at the free surface (top snapshots) and through the metasurface (bottom snapshots), filtered inside the band gap. As already revealed by the experimental results, when SH wave fronts impinge on the resonators, they are scattered and attenuated. The reverse-concavity wave front, a hallmark of wave reflection in front of the metasurface, detected in the experimental displacement field at $t_3 = 0.0312$ s, is numerically confirmed. The vertical cross section (A–A) cuts through the middle of the model [Fig. 3(d)], demonstrating the SH-wave propagation with and without the metasurface. In the vicinity of the resonant frequency of the oscillators, the part of the SH waves that is not reflected by the metasurface is driven under

the resonators, leading to a strong wave attenuation at the surface.

D. Effect of the grading

To investigate a possible shear-wave mode conversion enhanced by a graded metasurface, as observed for Rayleigh waves [24], we analyze the data recorded with metasurfaces of increasing and decreasing frequency with respect to the propagation direction. Figure 4(a) shows an outline of the two configurations. We compare the particle velocities, measured along the middle line of the box, in the frequency domain. In the decreasing-frequency case [Fig. 4(b)], waves are progressively reflected by the mechanical oscillators and the band gap is enlarged exactly as for the “classic metawedge” case described in Ref. [24]. Conversely, in the increasing-frequency case [Fig. 4(c)], the SH-wave energy is attenuated in a frequency range that shifts gradually toward higher values as the resonance of the mechanical oscillators increases.

This latter configuration (i.e., a graded resonant metasurface with increasing frequency) is implemented in the time domain for the experimental setup using SPEC-FEM3D. The computational domain, depicted in Fig. 5(c), is the same as the one adopted in Fig. 3(b). The line source, situated at a distance of 0.2 m from the left boundary, generates harmonic SH waves. We use a tapered sinusoidal signal to avoid spurious oscillations at the onset. The graded metasurface is modeled by varying the resonant frequency of the oscillators from 280 to 490 Hz. An analogous 3D model without the metasurface is used as the reference case [see Fig. 5(a)]. Time-transient 3D simulations are performed for different input-signal frequencies (350 and 370 Hz) with and without the resonators. The displacement field of the harmonic SH waves is shown in Fig. 5(b)

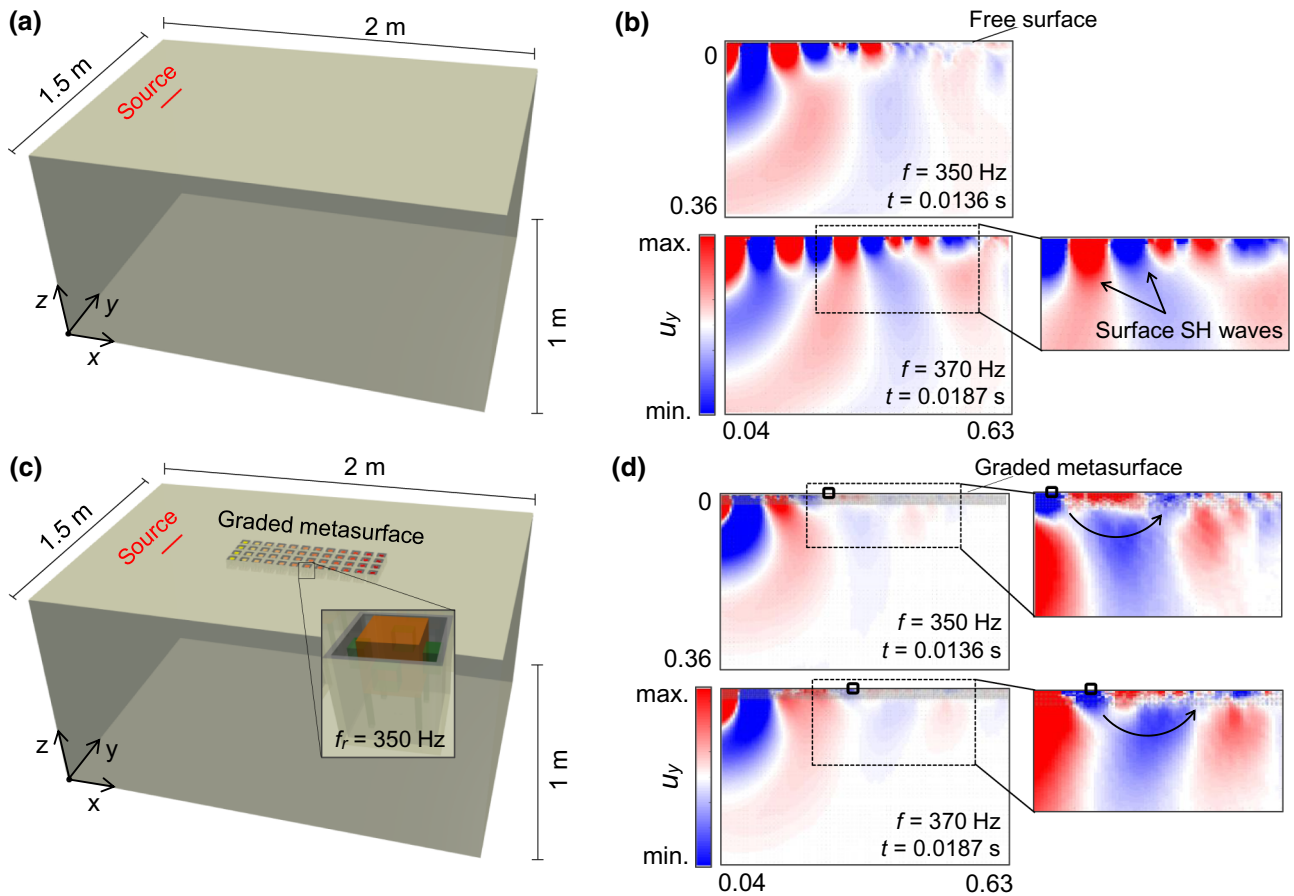


FIG. 5. Full-scale time-domain numerical simulations. (a) The computational domain modeled for the reference case characterized by the granular substrate excited by a harmonic line source (350 and 370 Hz). (b) The displacement field of harmonic SH waves traveling at the free surface of the granular substrate at two different excitation frequencies (350 and 370 Hz). (c) The computational domain characterized by the granular substrate and the graded metasurface excited by a harmonic line source (350 and 370 Hz). (d) The displacement field of harmonic SH waves traveling through the graded metasurface at two different excitation frequencies (350 and 370 Hz).

for the reference case and in Fig. 5(d) for the case of the graded metasurface. In the graded metasurface, the SH wave travels undisturbed until it reaches the resonator with a matching resonant frequency. At this position, dubbed the “turning point” (black small square), both at 350 Hz and at 370 Hz, the wave front separates from the surface. While the first-order mode hybridizes with the resonator (SH_{1m}), the second one (SH_{2m}) exhibits its maximum horizontal displacement underneath the resonator [inset of Fig. 2(b)]. However, after a short distance, the wave front returns to the surface. The lack of hybridization of the higher-order SH mode with the resonator, hybridization being prevented by the continuous variation of the shear and longitudinal velocity profile, allows the return of the wave front to the surface. Although the surface-to-body wave-conversion phenomenon does not occur, it is important to point out how the wave intensity is attenuated after encountering the resonant units.

III. CONCLUSIONS

In this work, we numerically and experimentally investigate the dynamics and the dispersion properties of shear horizontal waves localized at the surface of a granular medium and their interaction with local resonances. For the reference case (the pristine granular material without the resonators), the numerical model reveals an infinite number of SH modes, in alignment with recent analytical studies [33,34]; however, only the first two low-order modes are detected experimentally. When SH waves approach the resonant metasurface, a hybridization occurs between the fundamental mode and the mechanical oscillators and a frequency zone of quasizero surface velocity arises in the spectrum from 330 to 500 Hz. This attenuation zone is confirmed by the numerical-dispersion analysis, which indicates quasizero displacement in the surface layer including the resonant structures at the considered frequency range. As soon as the waves impinge on the resonators, they

are both backscattered and steered downward, channeled between the metasurface lower boundary and the in-depth stiffer medium.

Subsequently, we investigate the effect of a graded metasurface by spatially increasing or decreasing the resonant frequency of the oscillators. Unlike the mechanism observed in a bilayered medium [30], SH waves localized at the surface of a power-law elastic profile material are not steered into the bulk but remain confined at the surface. Although, at the “turning point,” the wave front detaches from the surface and is reoriented toward the interior of the substrate, after traveling a short distance it returns to the surface. The depth-increasing stiffness profile of the granular medium prevents the hybridization of the higher-order SH modes, inhibiting the surface-to-shear conversion mechanism.

Similar results may be achieved in other natural or artificial materials that feature an inhomogeneous power-law elastic profile, such as stratified soils at the seismic scale [44]. Although large-scale experiments are needed to establish the efficiency of these resonant metastructures, the findings can be used as a starting point for the study of more refined engineered devices for shear-wave attenuation in heterogeneous substrates. More sophisticated designs could, for instance, explore the adoption of nonlinear kinematics and inertial amplification mechanisms [45] to improve the dynamic-response bandwidth of the resonators.

ACKNOWLEDGMENTS

This research was partially supported by the Ambizione Fellowship Grant No. PZ00P2-174009 to A.C. and the ETH Research Grant No. 49 17-1 to E.C.

[1] J. B. Pendry, A. J. Holden, W. J. Stewart, and I. Youngs, Extremely Low Frequency Plasmons in Metallic Mesostuctures, *Phys. Rev. Lett.* **76**, 4773 (1996).

[2] J. B. Pendry, A. J. Holden, D. J. Robbins, and W. J. Stewart, Magnetism from conductors and enhanced nonlinear phenomena, *IEEE Trans. Microw. Theory Tech.* **47**, 2075 (1999).

[3] G. Ma and P. Sheng, Acoustic metamaterials: From local resonances to broad horizons, *Sci. Adv.* **2**, e1501595 (2016).

[4] R. V. Craster and S. Guenneau, *Acoustic Metamaterials: Negative Refraction, Imaging, Lensing and Cloaking* (Springer, London, 2012).

[5] M. I. Hussein, M. J. Leamy, and M. Ruzzene, Dynamics of phononic materials and structures: Historical origins, recent progress, and future outlook, *Appl. Mech. Rev.* **66**, 040802 (2014).

[6] R. Craster and S. Guenneau, *World Scientific Handbook of Metamaterials and Plasmonics: Elastic, Acoustic, and Seismic Metamaterials* (World Scientific, Singapore, 2018).

[7] V. K. Dertimanis, I. A. Antoniadis, and E. N. Chatzi, Feasibility analysis on the attenuation of strong ground motions using finite periodic lattices of mass-in-mass barriers, *J. Eng. Mech.* **142**, 04016060 (2016).

[8] Z. Liu, X. Zhang, Y. Mao, Y. Y. Zhu, Z. Yang, C. T. Chan, and P. Sheng, Locally resonant sonic materials, *Science* **289**, 1734 (2000).

[9] P. A. Deymier, *Acoustic Metamaterials and Phononic Crystals* (Springer, Berlin, 2013).

[10] Y. Liu and X. Zhang, Metamaterials: A new frontier of science and technology, *Chem. Soc. Rev.* **40**, 2494 (2011).

[11] L. D’Alessandro, E. Belloni, R. Ardito, F. Braghin, and A. Corigliano, Mechanical low-frequency filter via modes separation in 3D periodic structures, *Appl. Phys. Lett.* **111**, 231902 (2017).

[12] S. Brûlé, E. H. Javelaud, S. Enoch, and S. Guenneau, Experiments on Seismic Metamaterials: Molding Surface Waves, *Phys. Rev. Lett.* **112**, 133901 (2014).

[13] G. Finocchio, O. Casablanca, G. Ricciardi, U. Alibrandi, F. Garesci, M. Chiappini, and B. Azzarboni, Seismic metamaterials based on isochronous mechanical oscillators, *Appl. Phys. Lett.* **104**, 191903 (2014).

[14] R. Zhu, X. N. Liu, G. K. Hu, C. T. Sun, and G. L. Huang, A chiral elastic metamaterial beam for broadband vibration suppression, *J. Sound Vib.* **333**, 2759 (2014).

[15] M. Nouh, O. Aldraihem, and A. Baz, Vibration characteristics of metamaterial beams with periodic local resonances, *J. Vib. Acoust.* **136**, 061012 (2014).

[16] Y. Xiao, J. Wen, and X. Wen, Sound transmission loss of metamaterial-based thin plates with multiple subwavelength arrays of attached resonators, *J. Sound Vib.* **331**, 5408 (2012).

[17] M. Nouh, O. Aldraihem, and A. Baz, Wave propagation in metamaterial plates with periodic local resonances, *J. Sound Vib.* **341**, 53 (2015).

[18] E. Baravelli and M. Ruzzene, Internally resonating lattices for bandgap generation and low-frequency vibration control, *J. Sound Vib.* **332**, 6562 (2013).

[19] S. Krödel, N. Thoméa, and C. Daraio, Wide band-gap seismic metastructures, *Extreme Mech. Lett.* **4**, 111 (2015).

[20] A. Palermo, S. Krödel, K. H. Matlack, R. Zaccherini, V. K. Dertimanis, E. N. Chatzi, A. Marzani, and C. Daraio, Hybridization of Guided Surface Acoustic Modes in Unconsolidated Granular Media by a Resonant Metasurface, *Phys. Rev. Appl.* **9**, 054026 (2018).

[21] V. La Salandra, M. Wenzel, O. S. Bursi, G. Carta, and A. B. Movchan, Conception of a 3D metamaterial-based foundation for static and seismic protection of fuel storage tanks, *Front. Mater.* **4**, 30 (2017).

[22] O. Casablanca, G. Ventura, F. Garesci, B. Azzarboni, B. Chiaia, M. Chiappini, and G. Finocchio, Seismic isolation of buildings using composite foundations based on metamaterials, *J. Appl. Phys.* **123**, 174903 (2018).

[23] A. Casalotti, S. El-Borgi, and W. Lacarbonara, Metamaterial beam with embedded nonlinear vibration absorbers, *Int. J. Nonlinear Mech.* **98**, 32 (2018).

[24] A. Colombi, D. Colquitt, P. Roux, S. Guenneau, and R. V. Craster, A seismic metamaterial: The resonant metawedge, *Sci. Rep.* **6**, 27717 (2016).

- [25] A. Colombi, R. V. Craster, D. Colquitt, Y. Achaoui, S. Guenneau, P. Roux, and M. Rupin, Elastic wave control beyond band-gaps: Shaping the flow of waves in plates and half-spaces with subwavelength resonant rods, *Front. Mech. Eng.* **3**, 10 (2017).
- [26] A. A. Maznev and V. E. Gusev, Waveguiding by a locally resonant metasurface, *Phys. Rev. B* **92**, 115422 (2015).
- [27] M. Addouche, M. A. Al-Lethawe, A. Elayouch, and A. Khelif, Subwavelength waveguiding of surface phonons in pillars-based phononic crystal, *AIP Adv.* **4**, 124303 (2014).
- [28] D. J. Colquitt, A. Colombi, R. V. Craster, P. Roux, and S. R. L. Guenneau, Seismic metasurfaces: Sub-wavelength resonators and Rayleigh wave interaction, *J. Mech. Phys. Solids* **99**, 379 (2017).
- [29] A. Palermo and A. Marzani, Control of Love waves by resonant metasurfaces, *Sci. Rep.* **8**, 7234 (2018).
- [30] A. Maurel, J.-J. Marigo, K. Pham, and S. Guenneau, Conversion of Love waves in a forest of trees, *Phys. Rev. B* **98**, 134311 (2018).
- [31] J. D. Achenbach and O. Balogun, Anti-plane surface waves on a half-space with depth-dependent properties, *Wave Motion* **47**, 59 (2010).
- [32] L. Bodet, A. Dhemaied, R. Martin, R. Mourgues, F. Rejiba, and V. Tournat, Small-scale physical modeling of seismic-wave propagation using unconsolidated granular media, *Geophysics* **79**, T323 (2014).
- [33] V. Aleshin, V. Gusev, and V. Tournat, Acoustic modes propagating along the free surface of granular media, *J. Acoust. Soc. Am.* **121**, 2600 (2007).
- [34] V. E. Gusev, V. Aleshin, and V. Tournat, Acoustic Waves in an Elastic Channel near the Free Surface of Granular Media, *Phys. Rev. Lett.* **96**, 214301 (2006).
- [35] H. A. Makse, N. Gland, D. L. Johnson, and L. Schwartz, Granular packings: Nonlinear elasticity, sound propagation, and collective relaxation dynamics, *Phys. Rev. E* **70**, 061302 (2004).
- [36] G. Gazetas, Vibrational characteristics of soil deposits with variable wave velocity, *Int. J. Numer. Anal. Methods* **6**, 1 (1982).
- [37] P. Dakoulas and G. Gazetas, A class of inhomogeneous shear models for seismic response of dams and embankments, *Int. J. Soil Dyn. Earthquake Eng.* **4**, 166 (1985).
- [38] C. H. Liu and S. R. Nagel, Sound in Sand, *Phys. Rev. Lett.* **68**, 2301 (1992).
- [39] X. Jacob, V. Aleshin, V. Tournat, P. Leclaire, W. Lauriks, and V. E. Gusev, Acoustic Probing of the Jamming Transition in an Unconsolidated Granular Medium, *Phys. Rev. Lett.* **100**, 158003 (2008).
- [40] L. Bodet, X. Jacob, V. Tournat, R. Mourgues, and V. Gusev, Elasticity profile of an unconsolidated granular medium inferred from guided waves: Toward acoustic monitoring of analogue models, *Tectonophysics* **496**, 99 (2010).
- [41] S. Pasquet, L. Bodet, Q. Vitale, F. Rejiba, R. Guérin, R. Mourgues, and V. Tournat, Laser-Doppler acoustic probing of granular media with varying water levels, *Physics Procedia* **70**, 799 (2015).
- [42] V. Tournat, V. Zaitsev, V. Gusev, V. Nazarov, P. Béquin, and B. Castagnède, Probing Weak Forces in Granular Media through Nonlinear Dynamic Dilatancy: Clapping Contacts and Polarization Anisotropy, *Phys. Rev. Lett.* **92**, 85502 (2004).
- [43] A. S. Phani, J. Woodhouse, and N. A. Fleck, Wave propagation in two-dimensional periodic lattices, *J. Acoust. Soc. Am.* **119**, 1995 (2006).
- [44] L. Y. Faust, Seismic velocity as a function of depth and geologic time, *Geophysics* **16**, 192 (1951).
- [45] F. Zeighami, A. Palermo, and A. Marzani, Inertial amplified resonators for tunable metasurfaces, *Meccanica* **54**, 2053 (2019).